Journal of Photochemistry & Photobiology, B: Biology 183 (2018) 184–190

Contents lists available at ScienceDirect

Journal of Photochemistry & Photobiology, B: Biology

journal homepage: www.elsevier.com/locate/jphotobiol

Target-oriented photofunctional nanoparticles (TOPFNs) for selective photodynamic inactivation of *Methicillin-resistant Staphylococcus aureus* (MRSA)

Kang-Kyun Wang[a], Eon Pil Shin[a], Hye-Jin Lee[b], Seung-Jin Jung[a], Jeong-Wook Hwang[a], Il Heo[a], Jong-Ho Kim[a], Min-Kyu Oh[b,*], Yong-Rok Kim[a,*]

[a] Department of Chemistry, Yonsei University, Seoul 03722, Republic of Korea
[b] Department of Chemical and Biological Engineering, Korea University, Seoul 02841, Republic of Korea

ARTICLE INFO

Keywords:
Target-oriented photofunctional nanoparticles (TOPFNs)
Photodynamic inactivation (PDI)
Reactive oxygen species (ROS)
Methicillin-resistant *Staphylococcus aureus* (MRSA)

ABSTRACT

To inactivate methicillin-resistant *Staphylococcus aureus* (MRSA) with minimum damage to host cells and tissue, target-oriented photofunctional nanoparticles (TOPFNs) were fabricated and characterized. MRSA is a predominant infective pathogen even in hospital and non-hospital environments due to its ability to develop high levels of resistance to several classes of antibiotics through various pathways. To solve this major problem, photodynamic inactivation (PDI) method applies to treat antibiotic-resistant bacteria. PDI involves the photosensitizer (PS) and light with a specific wavelength to be able to apply for a non-invasive therapeutic procedure to treat pathogenic bacteria by inducing apoptosis or necrosis of microorganisms. However, most current PDI researches have suffered from the instability of PDI agents in the biological environment due to the lack of selectivity and low solubility of PDI agents, which leads to the low PDI efficiency. In this study, the TOPFNs were fabricated by an esterification reaction to introduce hematoporphyrin (HP) and MRSA antibody to the surface of Fe_3O_4 nanoparticles. The TOPFNs were designed as dispersible PDI agent in biological condition, which was effectively used for selectively capturing and killing of MRSA. The capture efficiency TOPFNs was compared with PFNs as a negative control. The results showed that the capture efficiency of TOPFNs and PFNs was 95.55% and 6.43% in MRSA and L-929 cell mixed condition, respectively. And TOPFNs have a selective killing ability for MRSA with minimum damage to L-929 cells. Furthermore, PDI effect of TOPFNs was evaluated on the mice *in vivo* condition in order to check the possibility of practical medical application.

1. Introduction

Bacteria replicate very rapidly and evolve to survive in the presence of the antibiotics through different pathways, such as mutation, conjugation, recombination, transduction, and transformation [1–4]. Use of antibiotics for bacterial infections during therapy could accelerate the emergence of antibiotic resistant bacteria [5,6]. Even though pharmacological industries produced a number of new drugs and antibiotics in the last four decades, resistance to these drugs by many pathogenic bacteria has been increased [7,8]. Fast increasing of antibiotics resistant bacterial strains is one of the major problems in medical [9,10]. Especially, *Staphylococcus aureus* (*S. aureus*), which is a typical pathogen both within hospitals and in a non-hospital environment [11] and rapid emergence of resistant bacteria is occurring worldwide [12]. And methicillin-resistant *Staphylococcus aureus* (MRSA) is difficult to be completely treated because it has the ability to develop high levels of resistance to several classes of antibiotics and, even more, these strains show resistance to the latest emerging antibiotics [13]. The methicillin acts by inhibiting penicillin-binding proteins (PBPs) that are involved in the biosynthesis of peptidoglycan, which is made of glycan chains essential polymer surrounding the cell and resistant the intracellular pressure of several atmospheres [14]. Even *S. aureus* can resistant to not only methicillin but also other β-lactam antibiotics through the expression of a foreign PBP, which is resistant to the action of methicillin [15]. So, these MRSA were often resistant to other classes of antibiotics through different mechanisms and this led to the research for new antibiotics against these resistant strains. Surprisingly, 43.6% of *Staphylococcus aureus* isolates in the United Kingdom in 2005 was found to be MRSA [10]. Mortality attributed to MRSA bacteremia has been estimated to be 22% [16]. Therefore, it is desirable to develop alternative approaches to avoid the spread of antibiotic resistant bacteria strains because of the growing resistance of MRSA to conventional

* Corresponding authors.
E-mail addresses: mkoh@korea.ac.kr (M.-K. Oh), yrkim@yonsei.ac.kr (Y.-R. Kim).

https://doi.org/10.1016/j.jphotobiol.2018.04.037
Received 21 December 2017; Received in revised form 6 March 2018; Accepted 23 April 2018
Available online 24 April 2018
1011-1344/

antimicrobial agents. In this respect, various therapeutic methods as microwave induced, X-ray induced PDT, and sonodynamic therapy have newly been investigated [17–19]. As one of the alternative method is photodynamic inactivation (PDI) treatment to can be suggested to treat various pathogenic microorganisms. The PDI provides a potential therapeutic approach to treat antibiotic resistant bacteria. The benefits over antibiotics in clinical treatment include localized wound curing and minimal side effects, resistance, and toxicity [20]. There are many papers about killing pathogenic bacteria by using photosensitizer (PS) and specific wavelength of light on *in-vitro* condition [21–27]. However, *in vivo* PDI experiments have only demonstrated in a few papers [28]. Its major obstacle is lack of selectivity for the target microorganism [29]. The free radicals and singlet oxygen generated by non-selective PS cause non-specific damage to surrounding normal cells or tissues in circulation in the body [30]. So, the efficient PDI of bacteria is based on the concept that photosensitizer (PS) should be localized in the targeted bacteria, not in the surrounding host tissues, and then absorb the specific wavelength of light to generate reactive oxygen species (ROS) that are able to kill target bacteria [31]. Also, the poor solubility of PS in biological environments is another obstacle in PDI research. For example, rose bengal, which is a well-known photosensitizer to generating ROS, is strongly limited for using the PDI agents due to aggregate in aqueous solution. Therefore, there are many efforts to enhance solubility or dispersity of PS in aqueous condition by many researchers [32,33].

In this study, we report the therapeutic feasibility of the target-oriented photofunctional nanoparticles (TOPFNs) for the methicillin-resistant *Staphylococcus aureus* (MRSA). We fabricated the Fe_3O_4 nanoparticles which were extensively exploited in a medical field because of biocompatibility, low toxicity, dispersity in biological environment, and stability in suspension [34–37]. Also, the magnetism of Fe_3O_4 nanoparticles can easily be utilized for the collection of TOPFNs with external magnetics after the photodynamic treatment. The Fe_3O_4 nanoparticles were functionalized with HP (hematoporphyrin) and monoclonal MRSA antibody by the esterification reaction. These TOPFNs were used for investigating the feasibility of selectively capturing and killing MRSA *in vitro* and *in vivo* PDI experiment.

2. Materials and Methods

2.1. Fabrication of Target-oriented Photofunctional Nanoparticles (TOPFNs)

The photosensitizer, hematoporphyrin (HP, 99%), $FeCl_3{\cdot}6H_2O$ (98%), NaAc (99%), and polyethylene glycol (PEG, 1305–1595 M.W.) were purchased from Aldrich (St. Louis; USA). Magnetic nanoparticles (MNP, Fe_3O_4) were fabricated using the solvothermal reduction method reported previously [38]. $FeCl_3{\cdot}6H_2O$ (1.35 g) and polyethylene glycol (1.0 g) were dissolved in ethylene glycol (40 mL) to form a clear solution, and then NaAc (4.69 g) was added to the mixture under vigorous stirring for 30 min at 60 °C. As-formed viscous slurry was transferred into a teflon-lined stainless-steel autoclave of 50 mL capacity. The autoclave was heated to and maintained at 200 °C for 12 h, and then naturally cooled down to room temperature. The obtained black precipitates were collected after being washed with distilled water and absolute alcohol several times and dried at 60 °C for 6 h. In order to fabricate TOPFNs by the wet chemical process, fabricated MNPs were dispersed in the HP solution (10 mL, 1.6×10^{-5} M in THF). The mixture was agitated at room temperature for 24 h. The product was washed with THF solvent three times to remove the residual HP and then dried at 60 °C for 6 h. The collected 1 mg of photofunctional magnetic nanoparticles (PMN, Fe_3O_4@HP) were washed with PBS solution to remove an adsobed chemical. After washing, the PMNs were suspended in 1 mL of PBS solution [39,40]. The solution of PMNs (1 mg/mL, 1 mL, about 2.37×10^{10} particles/mL) was dissolved in 2 mL of conjugation solution with MRSA antibody (1 mg/mL, 20 μL), 1-ethyl-3-(3-dimethylamino-propyl) carbodiimide hydrochloride (EDAC, 6.44 mM, 100 μL) and sulfo-*N*-hydroxysuccinimide (NHS, 8.68 mM, 100 μL) The mixture was agitated at room temperature for 2 h in the dark. After the reaction, the mixture was placed on a magnet for 1 min and any unbound MRSA antibody in the supernatant was removed to another vial. The TOPFNs were washed with PBS (pH 7.4) for three times and suspended in the PBS (1 mL).

2.2. Characterization and Spectroscopy Measurements

Field-emission scanning electron microscopy (FE-SEM, 7800F, JEOL) was utilized to study the morphology of the MNPs. The crystallographic structure of the MNPs was investigated with a X-ray diffractometer (XRD, Ultima IV, Rigaku) working with Cu Kα radiation. To confirm the fabrication of TOPFNs, Infrared spectra were obtained by using a furrier transform infrared spectrophotometer (FT-IR, Impact 400, Nicolet). Absorption and emission spectra were obtained with a UV–Vis spectrophotometer (U-2900, Hitachi) and a spectrofluorometer (Hitachi, F-4500), respectively. In order to check the singlet oxygen generation from TOPFNs, singlet oxygen phosphorescence was directly measured with the time-resolved spectroscopic method. The Nd-YAG (surelite II-10, Continuum) pumped optical parametric oscillator laser (OPO plus, Continuum) was utilized as the excitation source (λ_{ex} = 500 nm) for the detection of time-resolved singlet oxygen phosphorescence. The phosphorescence signal was collected with a near-infrared photo-multiplier tube (H10330A; Hamamatsu) at an angle perpendicular to the excitation beam through cutoff (< 1000 nm; CVI) and the interference filters (1270 nm, Spectrogon) to avoid light scattering from the MNPs [41]. The signal was amplified and acquired by an amplifier (SR445A, Stanford Research Systems) and a 500 MHz digital oscilloscope (DS07052A, Agilent Technology) and transferred to a computer for further analysis.

2.3. Biological Assay

For *in vitro* photodynamic bactericidal effect of TOPFNs on bacteria, we used *methicillin-resistant Staphylococcus aureus* (MRSA, Korean Culture Center of Microorganisms (KCCM), ATCC33591) and L-929 cells (2.0×10^6 cells/mL). This strain was grown in Brain Heart Infusion (BHI, MD 21152, Sparks, USA) medium. The bacteria were cultured at 37 °C for 15 h. Then, the culture media were centrifuged and bacteria were washed with PBS solution. Bacteria concentrations were determined with UV–Vis spectrophotometer and confirmed by spreading bacteria on BAP (Blood Agar plate) and incubating them at 37 °C for 15 h, followed by colony counting [42]. The volume of PBS solution was adjusted to achieve a target concentration of bacteria, 10^5 CFU/mL.

Generally, the main goal of cytotoxicity testing is to assess the biocompatibility of biomaterial itself using mammalian cell culture system [43,44], because the test is useful in evaluating the toxicity of biomaterials and it provides a good way to screen biomaterials prior to *in vivo* tests. Therefore, newly fabricated biomaterial itself including degradable and non-degradable material is required to be evaluated for cytotoxicity regardless of the material functionality. Unlike other studies utilized in biological safety testing, cytotoxicity is not a pass/fail test. Therefore, we have tested the cytotoxicity of MMPs itself on L-929 cells using MTT assay according to the document of International standard (ISO 10993-5) [45].

In order to determine the bacteria capture efficiency of the TOPFNs, MRSA (1.0×10^5 CFU/mL, 0.5 mL) and L-929 (2.0×10^6 cells/mL, 0.5 mL) in RPMI media were mixed with the TOPFNs (500 μg/mL, 0.5 mL) or the PMNs (500 μg/mL, 0.5 mL) for 30 min, respectively. From the mixed solutions, each of the bacteria-captured particle complexes (TOPFNs and PMNs) were separated using a magnet to calculate the number of captured bacteria.

For photodynamic bactericidal effect of TOPFNs, a light-emitting diode (LED; λ_{max} = 517 nm, full width at half-maximum (FWHM) = 37.8 nm, 3.9 mW/cm^2) was used for irradiation light source

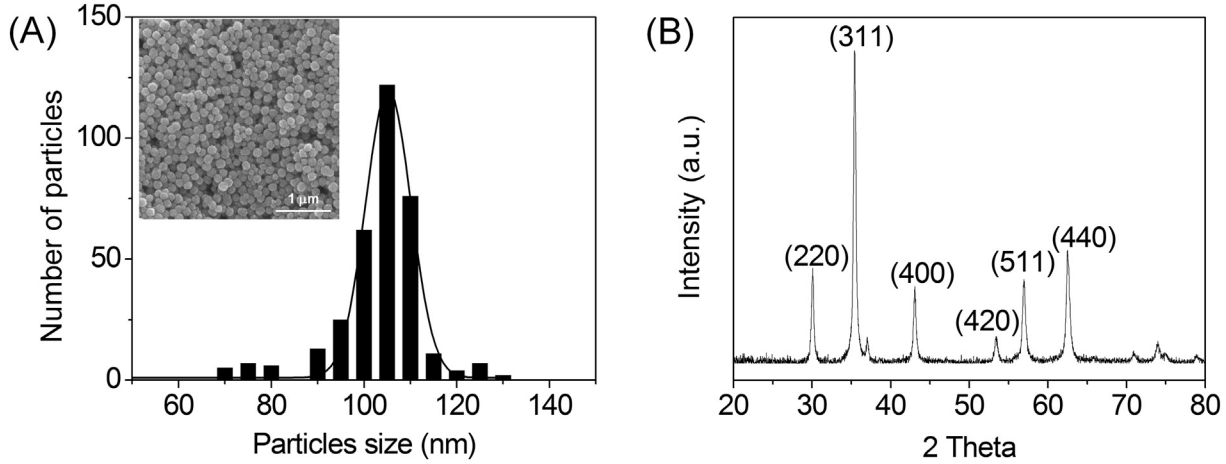

Fig. 1. (A) The size distribution and scanning electron microscope (SEM) image of the Fe_3O_4 nanoparticles (inset), (B) X-ray diffraction (XRD) pattern of the Fe_3O_4 nanoparticles.

with a cutoff filter (< 400 nm; CVI) to block the residual UV light of the LED. The power density of the LED light at sample position was measured with a power meter. TOPFNs (500 μg/mL, 0.5 mL) were added into the MRSA (1.0×10^5 CFU/mL, 0.5 mL) and L-929 (2.0×10^6 cells/mL, 0.5 mL) in RPMI media. After 30 min, the LED light radiated onto the mixture solution at various time intervals. After irradiation, the 100 μL of mixture solution was spread on a BAP and then incubated at 37 °C for 15 h in order to estimate the bactericidal effect of TOPFNs. And viability of live L-929 cells was checked by cell counting method using trypan blue staining protocol [46].

In order to check the possibility of practical application, the photodynamic bactericidal effect of TOPFNs was evaluated *in-vivo* experiment. The adult female mice (Charles River Laboratories Inc., USA), 5 weeks old and weighing 21–25 g, were used. All animal experimental procedures were approved by the Institutional Animal Care and Use Committee (IACUC) of Yonsei University (2012-0083) and all mice were maintained under the guidelines of an approved protocol. The mice were anesthetized with an intraperitoneal (i.p.) injection of ketamine/rompun. Back of mice was shaved and washed with saline solution. The skin on a back of mice was scratched with needles in the area of 1 cm^2. After 5 min, 10 μL of MRSA (10^{11} CFU/mL) in PBS containing LIVE/DEAD BacLight Bacterial Viability Kit was applied to a wounded skin on the back of mice for infection. The LIVE/DEAD Kit was included two components: SYTO9 stains the DNA with the green fluorescence in all bacteria, while propidium iodide (PI) provides intense red fluorescence [47]. The ratio of green and red fluorescence intensity of bacteria stained with this techniques allows the undamaged bacteria (with green fluorescence) to be distinguished from the damaged ones (with red and green fluorescence). DNA or RNA of undamaged bacteria are stained with only SYTO9 whereas DNA of damaged bacteria are stained with both SYTO9 and PI [48]. Therefore when bacterial cell membranes were damaged green fluorescence intensity is decreased due to the entrance of propidium iodide. After 30 min allows to MRSA binding host tissues [49]. TOPFNs were applied to the infected region of only mouse 2 and 3. The LED (λ_{max}: 517 nm, power density: 11.8 mW/cm^2) light irradiated to mouse 1 and 3 for 1 h, and fluorescence from a back of mice was measured with Luminescence and Fluorescence Animal Imaging System (IVIS 200, Xenogen) at every 10 min. Fluorescence intensities from the images were quantified using by Xenogen Living Image® software.

3. Results and Discussions

Novel target-oriented photofunctional MNPs were fabricated by surface functionalization of the magnetic nanoparticles with a photosensitizer, HP, and a targeting molecule, MRSA-antibody. The HP was bonded to transition metal cations on the surface of the Fe_3O_4 nanoparticles *via* an esterification reaction. In order to improve the targeting ability of the MNPs, MRSA-antibody was introduced to the surface of the MNPs. Fig. 1(A, inset) shows the morphological analysis of the Fe_3O_4 nanoparticles by FE-SEM which clearly indicated that nanoparticles were mostly spherical with good size uniformity. And Fig. 1(A) shows the size histogram of the Fe_3O_4 nanoparticles, which was estimated by sampling 300 particles in different regions of the FE-SEM image. It shows the nanoparticles size distribution, where the average diameter of $< \varphi > = 103 \pm 7$ nm was obtained using a Gaussian fit. Fig. 1(B) shows the XRD patterns of the powder Fe_3O_4 nanoparticles. The diffraction peaks from the Fe_3O_4 particles occur at Bragg angles of 30.0, 35.6, 43.3, 53.7, 57.0, and 62.8°. These Bragg reflection peaks were confirmed by their Miller indices ((220), (311), (400), (422), (511), and (440)) that was obtained from the standard Fe_3O_4 powder diffraction data (JCPDS, card 19-0629). All the strong diffraction peaks can be indexed to a typical magnetite crystal with cubic inverse spinel structure [50,51].

To understand the bonding properties of the HP and MRSA antibody to the surface of the MNPs, FT-IR spectra of HP, PMNs, MRSA-antibody, and TOPFNs were compared, as shown in Fig. 2. The IR spectrum of

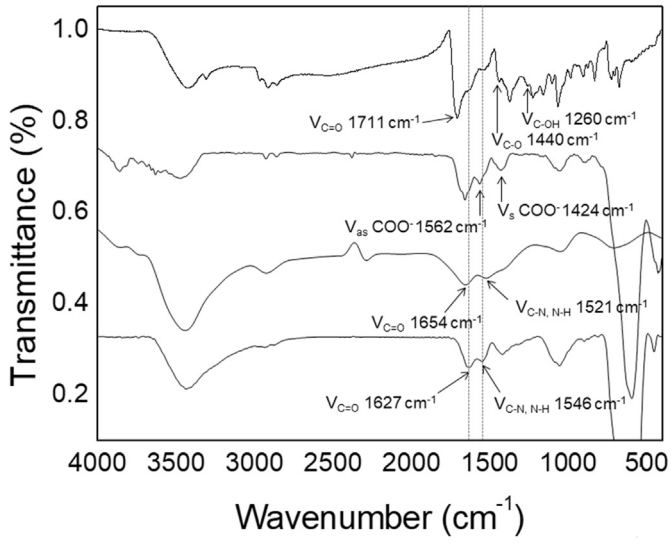

Fig. 2. FT-IR spectra of (A) HP, (B) HP@Fe_3O_4, (C) MRSA antibody, (D) TOPFNs.

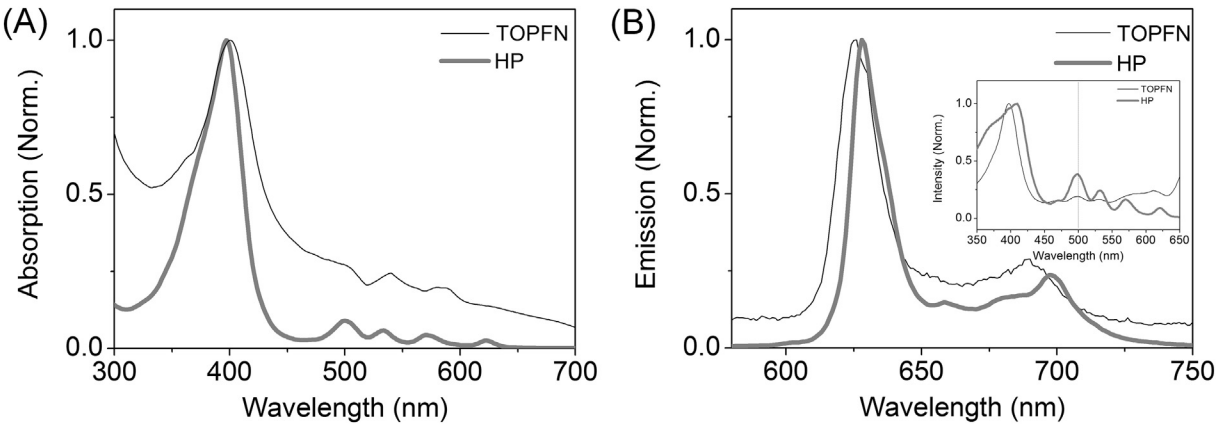

Fig. 3. (A) Absorption and (B) emission spectra of pure HP and TOPFNs in EtOH. The excitation wavelength is 500 nm for the emission spectra. The inset of (B) shows the excitation spectra of pure HP and TOPFN at the emission wavelength of 687 nm.

pure HP presents absorption peaks at 1711 cm^{-1}, 1440 cm^{-1}, and 1260 cm^{-1}, which correspond to the stretching modes of the free carbonyl double bond ($\nu_{C=O}$), the carbon-oxygen single bond (ν_{C-O}), and the OH deformation (ν_{C-OH}), respectively [52]. These characteristic absorption peaks suggest that pure HP has protonated carboxyl groups (COOH), as expected. After the conjugation reaction occurs between the carboxyl group and the Fe ion, the IR spectrum of the HP bonded to surface of Fe_3O_4 presents the peaks corresponding to the protonated carboxyl group, and the new bands appear at 1562 cm^{-1} and 1424 cm^{-1}, which are ascribed to the asymmetric (ν_{as}) and the symmetric (ν_s) stretch vibrations of the carboxylate group, respectively [53,54]. The peaks of MRSA antibody in the spectrum are assigned to be the C═O stretching mode of the amide I group at 1654 cm^{-1}, the C—N stretching and N—H bending vibrational modes of amide II at 1521 cm^{-1} from the reference [55]. In the spectrum of MRSA antibody bounded HP@ Fe_3O_4, the C=O stretching mode peak and the C—N stretching and N—H bending vibrational modes peak of MRSA antibody are shifted to 1627 and 1546 cm^{-1} due to the Maillard reaction between carboxylic groups (—COOH) of HP@Fe_3O_4 and amide groups ($-NH_2$) of MRSA antibody [56]. Therefore, these results suggest that HP and MRSA antibody molecules are bound up with the surface of Fe_3O_4 nanoparticle coating through the carboxyl and amide group, respectively.

The spectrum of HP in ethanol solution shows one B band (400 nm) and four Q bands (500, 533, 573, and 625 nm) as shown in Fig. 3(A). The absorption spectrum of TOPFNs in ethanol solution also includes the B and Q bands at similar wavelengths but with broader shapes and slightly red shifted peak positions. Such difference in the peak width and position is possibly due to the self-coupling of HPs attached to the surface and the inhomogeneous bonding nature of HP to the surface of TOPFNs [57]. The fluorescence emission peaks of TOPFNs in ethanol solution at 623 and 687 nm were also similar to those of HP in ethanol solution at the excitation of 500 nm but with slightly blue shifted peaks positions as shown in Fig. 3(B). Such blue shift suggests that a strong coupling exists between HP and the surface of the magnetic nanoparticle [38]. In order to specify the optical property at the excitation wavelength, excitation spectra of TOPFN and HP were measured at the emission wavelength (687 nm). As shown in Fig. 3(B, inset), the samples were optically matched at the excitation wavelength (500 nm). In order to estimate the amount of introduced HP on the surface of the magnetic particles, the comparative absorption ODs at 500 nm was measured with the reference HP solution (4.28×10^{-2} mM) before the insertion of the magnetic particles for reaction and the remaining HP solution obtained after the reaction with the particles [38]. The result of O.D. difference indicates that 2.86×10^{-8} mol (equivalent to 1.72×10^{16} molecules) of HP are immobilized onto the surface of 1 mg of magnetic particles.

The most direct measurement method for singlet oxygen is the detection of phosphorescence from the deactivation of singlet oxygen molecules induced by photoexcited HP. As shown in Fig. 4, singlet oxygen phosphorescence signals from HP and TOPFNs were measured in ethanol solution at a detection wavelength of 1270 nm which is the maximum of the phosphorescence emission. The intensities of the singlet oxygen phosphorescence signal at the zero time point were nearly identical for HP and TOPFNs. The phosphorescence decay signals from HP and TOPFNs were fitted to a single exponential function,

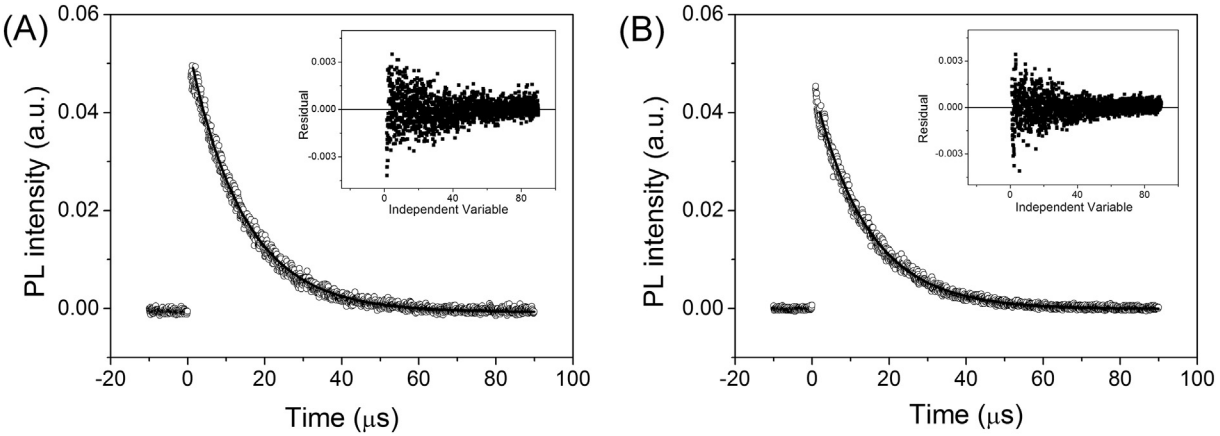

Fig. 4. Phosphorescence decay signals induced by relaxation of the singlet oxygen from (A) HP, and (B) TOPFN in ethanol solution (The insets are residuals of fitting function). Phosphorescence signals were detected at 1270 nm and fitted with a single exponential function (solid line).

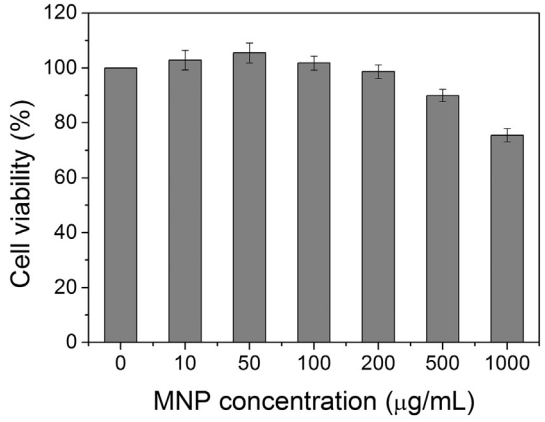

Fig. 5. The cytotoxicity of TOPFNs itself to L-929 cells incubated with various concentrations of TOPFNs for 24 h at 37 °C in 100% humidity and 5% CO_2 in the dark.

yielding similar singlet oxygen lifetimes of 14.3 and 14.1 μs, respectively. These measured singlet oxygen lifetimes are consistent with the reported value [57,58]. These results suggest that the singlet oxygen generated from TOPFNs did not quenched by the MNP and MRSA antibody on the surface of MNPs.

The cytotoxicity of TOPFNs itself to L-929 cells was evaluated using the MTT assay. The MTT was assessed using the CellTiter 96 Aqueous One Solution Cell Proliferation Assay kit (Promega, WI, USA), and measured optically at 490 nm. As shown in Fig. 5, the data indicate no cytotoxicity of TOPFNs itself in the concentration range of 0–500 μg/mL, that are the utilized range for the photodynamic inactivation of bacteria in this study. Cell viabilities are > 90%. The low-cytotoxicity of TOPFNs is expected to be due to the large particle size of 100 nm that does not affect to the cell viability. It has been reported that the penetration possibility is very low for the nanoparticle that has the size larger than 70 nm [59,60].

The MRSA capture efficiency of the TOPFNs was compared with PMNs as a negative control. As shown in Fig. 6(A), the bacteria capture efficiency of TOPFNs and PMNs were 95.55 ± 2.49% and 6.43 ± 1.96% of the original number of bacteria, respectively. As expectation, the TOPFNs exhibited high capture efficiency for MRSA, while PMNs didn't show a significant value due to non-specific bonding sites for the adsorption of MRSA on the surface. The results show the more enhanced capturing efficiency than the previous reports [61,62]. The viability of MRSA was not changed by the TOPFNs itself at the same time. Also, viabilities of L-929 cells were not changed in the light irradiation condition because L-929 cells had not been reacted with irradiated light [63]. In particular, the TOPFNs in MRSA and L-929 cells mixture solution were irradiated with LED system with a 3.93 mW/cm^2 for 60 min. After the irradiation, we evaluated a viability of MRSA and L-929 cell at every 10 min to demonstrate the selective PDI efficiency. The results were shown in Fig. 6(B). The viability of MRSA was dramatically dropped from 1.0×10^5 CFU/mL to 10^0 CFU/mL in 60 min. But the viability of live L-929 cells is nearly not affected by the ROS in this experimental condition. The results suggest that the TOPFNs can be used appropriately for PDI agent minimizing damages to surrounding normal cells and maxmizing PDI efficiency to the targeted bacteria.

Fig. 7 shows the bactericidal activity during *in vivo* PDI treatment. The TOPFNs were applied to the scratched wound on a back skin infected with MRSA of mice. All mice (1–3) were infected with MRSA in the defined area on the back of the mouse. The MRSA-infected wound of the mice (2) and (3) were applied with the TOPFNs, while mouse (1)

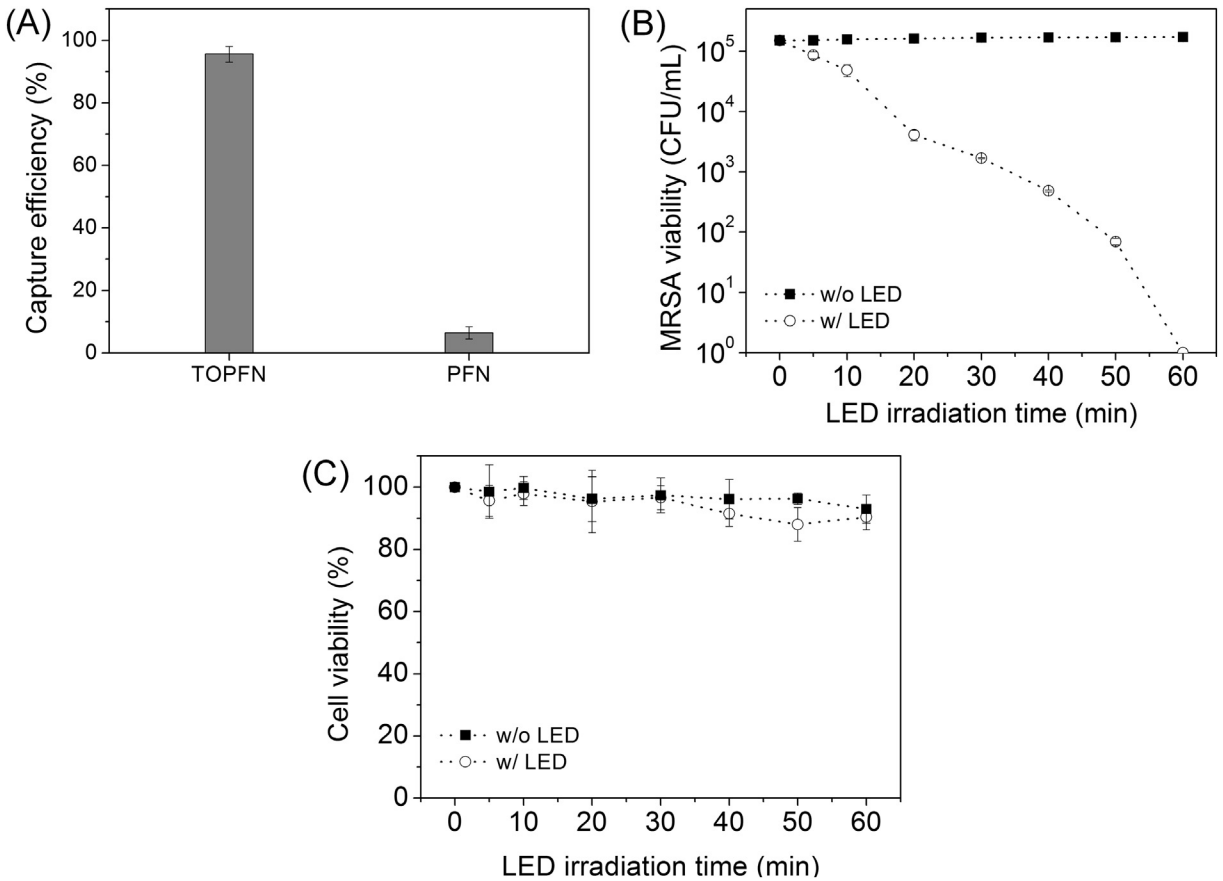

Fig. 6. (A) The MRSA capture efficiency of TOPFNs and PMNs and (B) Survival curves of MRSA and (C) L-929 cells in MRSA and L-929 cells mixture solution with TOPFNs.

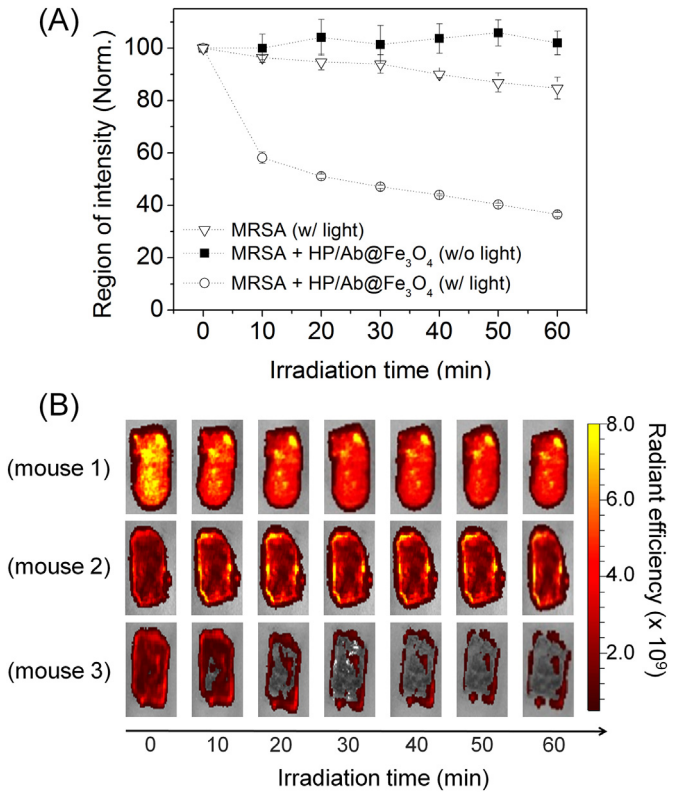

Fig. 7. *In vivo* PDI using TOPFNs for MRSA-infected mice. (A) The quantified results of ROI (region of intensity) for a 1 × 1 cm^2 area. (B) Successive fluorescent images of the skin on a back of mice infected with MRSA during the PDI experiment.

was not as a control. To confirm the efficacy of PDI, the back of the mice (1) and (3) was irradiated with LED. The mouse (2) was kept in the dark container as a dark control group. And then we acquired the successive fluorescence images from a back of mice every 10 min during LED irradiation. The ROI intensities of the mouse (1) and mouse (2) were slightly decreased and not changed, respectively. It means that viability of MRSA is maintained as the similar value of the initial concentration of MRSA at the infection area since it is difficult for the captured MRSA to diffuse into the dermis from the epidermis of a mouse. Therefore, the TOPFNs depresses the diffusion effect of MRSA into other tissue by capturing MRSA. In the case of the mouse (1), we assume that it may be a result of diffusion of MRSA into the dermis from the wounded epidermis of a mouse. In the case of the mouse (3) applied with TOPFNs under light irradiation, MRSA infection rate was significantly down to 38% for 60 min.

4. Conclusions

In conclusion, a goal of our work is treating methicillin-resistant *Staphylococcus aureus* (MRSA) by photodynamic inactivation (PDI) accompanied with minimizing damage to the host tissues. We fabricated target-oriented photofunctional nanoparticles (TOPFNs), which are Fe_3O_4 nanoparticles conjugated with both hematoporphyrin (HP) and monoclonal MRSA antibody. It is biocompatible and has original functionality which of generating ROS and capturing MRSA. Our results show that the TOPFNs killed selectively MRSA in L-929 cells mixed *in vitro* condition. And the PDI effect of TOPFNs was confirmed *in vivo* experiment condition. The results suggest that he TOPFNs can be used for treating antibiotic-resistant bacteria under a specific wavelength of light instead of using antibiotics or drugs which may cause to emerge antibiotic resistant bacteria. And it can be applied to a new strategy to cure antibiotic resistant microbial disease.

Acknowledgments

K.K. Wang, E.P. Shin, H. J. Lee and S. J. Jung contributed equally to this manuscript. This work was supported by the National Research Foundation of Korea (NRF) grant funded by the Korea government (MSIP) (No. NRF-2017R1A5A1015365, No. NRF-2016R1A2B4011155) and Cooperative Research Program for Agriculture Science & Technology Development (Project No. PJ01083001), Rural Development Administration (PJ1083001), Republic of Korea.

Conflict of Interests

The authors declare that there is no conflict of interests regarding the publication of this paper.

References

[1] S.N. Cohen, A.C. Chang, L. Hsu, Nonchromosomal antibiotic resistance in bacteria: genetic transformation of *Escherichia coli* by R-factor DNA, Proc. Natl. Acad. Sci. U. S. A. 69 (1972) 2110–2114.
[2] D.I. Andersson, Persistence of antibiotic resistant bacteria, Curr. Opin. Microbiol. 6 (2003) 452–456.
[3] B.R. Levin, V. Perrot, N. Walker, Compensatory mutations, antibiotic resistance and the population genetics of adaptive evolution in bacteria, Genetics 154 (2000) 985–997.
[4] M. Steinmetz, R. Richter, Plasmids designed to alter the antibiotic-resistance expressed by insertion mutations in bacillus-subtilis, through in-vivo recombination, Gene 142 (1994) 79–83.
[5] P. Montravers, R. Gauzit, C. Muller, J.P. Marmuse, A. Fichelle, J.M. Desmonts, Emergence of antibiotic-resistant bacteria in cases of peritonitis after intraabdominal surgery affects the efficacy of empirical antimicrobial therapy, Clin. Infect. Dis. 23 (1996) 486–494.
[6] I. Chopra, A.J. O'Neill, K. Miller, The role of mutators in the emergence of antibiotic-resistant bacteria, Drug Resist. Updat. 6 (2003) 137–145.
[7] G.G.F. Nascimento, J. Locatelli, P.C. Freitas, G.L. Silva, Antibacterial activity of plant extracts and phytochemicals on antibiotic-resistant bacteria, Braz. J. Microbiol. 31 (2000) 247–256.
[8] A.A. El Solh, C. Pietrantoni, A. Bhat, M. Bhora, E. Berbary, Indicators of potentially drug-resistant bacteria in severe nursing home-acquired pneumonia, Clin. Infect. Dis. 39 (2004) 474–480.
[9] M.C.J. Bootsma, O. Diekmann, M.J.M. Bonten, Controlling methicillin-resistant Staphylococcus aureus: quantifying the effects of interventions and rapid diagnostic testing, Proc. Natl. Acad. Sci. U. S. A. 103 (2006) 5620–5625.
[10] P.M. Hawkey, The growing burden of antimicrobial resistance, J. Antimicrob. Chemother. 62 (2008) I1–I9.
[11] J. Lin, D. Lin, P. Xu, T. Zhang, Q. Ou, C. Bai, Z. Yao, Non-hospital environment contamination with Staphylococcus aureus and methicillin-resistant Staphylococcus aureus: proportion meta-analysis and features of antibiotic resistance and molecular genetics, Environ. Res. 150 (2016) 528–540.
[12] C.L. Ventola, The antibiotic resistance crisis: part 1: causes and threats, P & T 40 (2015) 277–283.
[13] J.L. Raygada, D.P. Levine, Methicillin-resistant *staphylococcus aureus*: a growing risk in the hospital and in the community, Am. Health Drug Benefits 2 (2009) 86–95.
[14] E. Sauvage, F. Kerff, M. Terrak, J.A. Ayala, P. Charlier, The penicillin-binding proteins: structure and role in peptidoglycan biosynthesis, FEMS Microbiol. Rev. 32 (2008) 234–258.
[15] P.D. Stapleton, P.W. Taylor, Methicillin resistance in *Staphylococcus aureus*: mechanisms and modulation, Sci. Prog. 85 (2002) 57–72.
[16] S.E. Cosgrove, Y.L. Qi, K.S. Kaye, S. Harbarth, A.W. Karchmer, Y. Carmeli, The impact of methicillin-resistance in Staphylococcus aureus bacteremia on patient outcomes: mortality, length of stay, and hospital charges, Infect. Cont. Hosp. Ep. 26 (2005) 166–174.
[17] C.L. Pan, M.H. Chen, F.I. Tung, T.Y. Liu, A nanovehicle developed for treating deep-seated bacteria using low-dose X-ray, Acta Biomater. 47 (2017) 159–169.
[18] X. Chu, K. Li, H. Guo, S. Shuda, X. Wang, J. Zhang, W. Chen, Y. Zhang, Exploration of graphite-C3N4 quantum dots for microwave-induced photodynamic therapy, ACS Biomater. Sci. Eng. 3 (2017) 1836–1844.
[19] X. Wang, M. Ip, A.W. Leung, C. Xu, Sonodynamic inactivation of methicillin-resistant Staphylococcus aureus in planktonic condition by curcumin under ultrasound sonication, Ultrasonics 54 (2014) 2109–2114.
[20] T.A. Skwor, S. Klemm, H.Y. Zhang, B. Schardt, S. Blaszczyk, M.A. Bork, Photodynamic inactivation of methicillin-resistant *Staphylococcus aureus* and *Escherichia coli*: a metalloporphyrin comparison, J. Photochem. Photobiol. B 165 (2016) 51–57.
[21] R. Dosselli, R. Millioni, L. Puricelli, P. Tessari, G. Arrigoni, C. Franchin, A. Segalla, E. Teardo, E. Reddi, Molecular targets of antimicrobial photodynamic therapy identified by a proteomic approach, J. Proteome 77 (2012) 329–343.
[22] D.E. Dolmans, D. Fukumura, R.K. Jain, Photodynamic therapy for cancer, Nat. Rev. Cancer 3 (2003) 380–387.
[23] J.L. Wardlaw, T.J. Sullivan, C.N. Lux, F.W. Austin, Photodynamic therapy against

common bacteria causing wound and skin infections, Vet. J. 192 (2012) 374–377.
[24] N. Kashef, G.R.S. Abadi, G.E. Djavid, Phototoxicity of phenothiazinium dyes against methicillin-resistant *Staphylococcus aureus* and multi-drug resistant *Escherichia coli*, Photodiagn. Photodyn. Ther. 9 (2012) 11–15.
[25] M. Veerapandian, L. Zhang, K. Krishnamoorthy, K. Yun, Surface activation of graphene oxide nanosheets by ultraviolet irradiation for highly efficient anti-bacterials, Nanotechnology 24 (2013) 395706 (11pp).
[26] T. Mthethwa, T. Nyokong, Photoinactivation of *Candida albicans* and *Escherichia coli* using aluminium phthalocyanine on gold nanoparticles, Photochem. Photobiol. Sci. 14 (2015) 1346–1356.
[27] S. Khan, S.N. Khan, R. Meena, A.M. Dar, R. Pal, A.U. Khan, Photoinactivation of multidrug resistant bacteria by monomeric methylene blue conjugated gold nanoparticles, J. Photochem. Photobiol. B Biol. 174 (2017) 150–161.
[28] M.F. Wu, M. Deichelbohrer, T. Tschernig, M.W. Laschke, N. Szentmary, D. Huttenberger, H.J. Foth, B. Seitz, M. Bischoff, Chlorin e6 mediated photodynamic inactivation for multidrug resistant *Pseudomonas aeruginosa* keratitis in mice in vivo, Sci. Rep. 7 (2017) 1–12.
[29] T. Iriuchishima, A. Saito, S. Aizawa, K. Taira, T. Yamamoto, J. Ryu, The minimum influences for murine normal joint tissue by novel bactericidal treatment and photodynamic therapy using Na-pheophorbide a for septic arthritis, Photomed. Laser Surg. 26 (2008) 153–158.
[30] C.H. Liu, W.S. Lee, W.C. Wu, Photodynamic inactivation against *Pseudomonas aeruginosa* by curcumin microemulsions, RSC Adv. 6 (2016) 63013–63022.
[31] A.A. Rosenkranz, D.A. Jans, A.S. Sobolev, Targeted intracellular delivery of photosensitizers to enhance photodynamic efficiency, Immunol. Cell Biol. 78 (2000) 452–464.
[32] L. Moczek, M. Nowakowska, Novel water-soluble photosensitizers from chitosan, Biomacromolecules 8 (2007) 433–438.
[33] M. Nowakowska, S. Zapotoczny, M. Sterzel, E. Kot, Novel water-soluble photosensitizers from dextrans, Biomacromolecules 5 (2004) 1009–1014.
[34] J.K. Xu, F.F. Zhang, J.J. Sun, J. Sheng, F. Wang, M. Sun, Bio and nanomaterials based on Fe_3O_4, Molecules 19 (2014) 21506–21528.
[35] S. Laurent, A.A. Saei, S. Behzadi, A. Panahifar, M. Mahmoudi, Superparamagnetic iron oxide nanoparticles for delivery of therapeutic agents: opportunities and challenges, Expert Opin. Drug Deliv. 11 (2014) 1449–1470.
[36] J. Estelrich, M.J. Sanchez-Martin, M.A. Busquets, Nanoparticles in magnetic resonance imaging: from simple to dual contrast agents, Inter. J. Nanomed. 10 (2015) 1727–1741.
[37] B. Kalska-Szostko, U. Wykowska, K. Piekut, D. Satuł, Stability of Fe_3O_4 nanoparticles in various model solutions, Colloids Surf. A Physicochem. Eng. Asp. 450 (2014) 15–24.
[38] K.H. Choi, H.J. Lee, B.J. Park, K.K. Wang, E.P. Shin, J.C. Park, Y.K. Kim, M.K. Oh, Y.R. Kim, Photosensitizer and vancomycin-conjugated novel multifunctional magnetic particles as photoinactivation agents for selective killing of pathogenic bacteria, Chem. Commun. 48 (2012) 4591–4593.
[39] M.L. Embleton, S.P. Nair, B.D. Cookson, M. Wilson, Selective lethal photosensitization of methicillin-resistant Staphylococcus aureus using an IgG-tin(IV) chlorin e6 conjugate, J. Antimicrob. Chemother. 50 (2002) 857–864.
[40] M.L. Embleton, S.P. Nair, B.D. Cookson, M. Wilson, Antibody-directed photodynamic therapy of methicillin resistant *Staphylococcus aureus*, Microb. Drug Resist. 10 (2004) 92–97.
[41] K.K. Wang, J. Li, B.J. Kim, J.H. Lee, H.W. Shin, S.H. Ko, W.Y. Lee, C.H. Lee, S.H. Jung, Y.R. Kim, Photophysical properties of pheophorbide-a derivatives and their photodynamic therapeutic effects on a tumor cell line in vitro, Int. J. Photoenergy (2014) 1–7.
[42] C.Y. Chen, G.W. Nace, P.L. Irwin, A 6 x 6 drop plate method for simultaneous colony counting and MPN enumeration of *Campylobacter jejuni*, *Listeria monocytogenes*, and *Escherichia coli*, J. Microbiol. Methods 55 (2003) 475–479.
[43] K. Keiser, C.C. Johnson, D.A. Tipton, Cytotoxicity of mineral trioxide aggregate using human periodontal ligament fibroblasts, J. Endodont. 26 (2000) 288–291.
[44] B. Ekwall, Screening of toxic compounds in mammalian-cell cultures, Ann. N. Y. Acad. Sci. 407 (1983) 64–77.
[45] K.C. Nam, K.H. Choi, K.D. Lee, J.H. Kim, J.S. Jung, B.J. Park, Particle size dependent photodynamic anticancer activity of hematoporphyrin-conjugated Fe_3O_4 particles, J. Nanomater. (2016) 1–9.
[46] D. Cadena-Herrera, J.E. Esparza-De Lara, N.D. Ramirez-Ibanez, C.A. Lopez-Morales, N.O. Perez, L.F. Flores-Ortiz, E. Medina-Rivero, Validation of three viable-cell counting methods: manual, semi-automated, and automated, Biotechnol. Rep. 7 (2015) 9–16.
[47] M. Berney, F. Hammes, F. Bosshard, H.U. Weilenmann, T. Egli, Assessment and interpretation of bacterial viability by using the LIVE/DEAD BacLight kit in combination with flow cytometry, Appl. Environ. Microbiol. 73 (2007) 3283–3290.
[48] S.M. Stocks, Mechanism and use of the commercially available viability stain, BacLight, Cytom. Part A 61A (2004) 189–195.
[49] T.H. Dai, G.P. Tegos, T. Zhiyentayev, E. Mylonakis, M.R. Hamblin, Photodynamic therapy for methicillin-resistant *Staphylococcus aureus* infection in a mouse skin abrasion model, Lasers Surg. Med. 42 (2010) 38–44.
[50] S.F. Chin, K.S. Iyer, C.L. Raston, Facile and green approach to fabricate gold and silver coated superparamagnetic nanoparticles, Cryst. Growth Des. 9 (2009) 2685–2689.
[51] K.H. Choi, K.K. Wang, E.P. Shin, S.L. Oh, J.S. Jung, H.K. Kim, Y.R. Kim, Water-soluble magnetic nanoparticles functionalized with photosensitizer for photocatalytic application, J. Phys. Chem. C 115 (2011) 3212–3219.
[52] B.J. Park, K.H. Choi, K.C. Nam, J. Min, K.D. Lee, H.S. Uhm, E.H. Choi, H.J. Kim, J.S. Jung, Photodynamic anticancer activity of $CoFe_2O_4$ nanoparticles conjugated with hematoporphyrin, J. Nanosci. Nanotechnol. 15 (2015) 7900–7906.
[53] N.Q. Wu, L. Fu, M. Su, M. Aslam, K.C. Wong, V.P. Dravid, Interaction of fatty acid monolayers with cobalt nanoparticles, Nano Lett. 4 (2004) 383–386.
[54] K.K. Wang, J.W. Jang, E.P. Shin, H.W. Song, J.W. Hwang, Y.K. Kim, C.S. Lim, Y.R. Kim, Eradication of plasmodium falciparum from erythrocytes by controlled reactive oxygen species via photodynamic inactivation coupled with photofunctional nanoparticles, ACS Appl. Mater. Interfaces 9 (2017) 12975–12981.
[55] L. Mocan, C. Matea, F.A. Tabaran, O. Mosteanu, T. Pop, C. Puia, L. Agoston-Coldea, D. Gonciar, E. Kalman, G. Zaharie, C. Iancu, T. Mocan, Selective in vitro photothermal nano-therapy of MRSA infections mediated by IgG conjugated gold nanoparticles, Sci. Rep. 6 (2016) 1–9.
[56] G. Liu, Q.X. Zhong, Glycation of whey protein to provide steric hindrance against thermal aggregation, J. Agric. Food Chem. 60 (2012) 9754–9762.
[57] K.K. Wang, M.S. Jung, K.H. Choi, H.W. Shin, S.I. Oh, J.E. Im, D.H. Kim, Y.R. Kim, Fabrication and photophysical properties of singlet oxygen generating nanoporous membrane, Surf. Coat. Technol. 205 (2011) 3905–3908.
[58] M.P. Samtsov, D.S. Tarasau, A.S. Stasheuski, K.N. Kaplevsky, E.S. Voropay, Concentration increase of the singlet-oxygen generation quantum yield by an Indotricarbocyanine dye, J. Appl. Spectrosc. 81 (2014) 214–221.
[59] W. Jiang, B.Y.S. Kim, J.T. Rutka, W.C.W. Chan, Nanoparticle-mediated cellular response is size-dependent, Nat. Lett. 3 (2008) 144–150.
[60] S. Sabella, R.P. Carney, V. Brunetti, M.A. Malvindi, N.A. Juffali, G. Vecchio, S.M. Janes, O.M. Bakr, R. Cingolani, F. Stellacci, P.P. Pompa, A general mechanism for intracellular toxicity of metal-containing nanoparticles, Nano 6 (2014) 7052–7061.
[61] M. Varshney, L. Yang, X.L. Su, Y. Li, Magnetic nanoparticle-antibody conjugates for the separation of *Escherichia coli* O157:H7 in ground beef, J. Food Prot. 68 (2005) 1804–1811.
[62] M.H. Kim, I. Yamayoshi, S. Mathew, H. Lin, J. Nayfach, S.I. Simon, Magnetic nanoparticle targeted hyperthermia of cutaneous *Staphylococcus aureus* infection, Ann. Biomed. Eng. 41 (2012) 598–609.
[63] A. Yoshida, H. Sasaki, T. Toyama, M. Araki, J. Fujioka, K. Tsukiyama, N. Hamada, F. Yoshino, Antimicrobial effect of blue light using *Porphyromonas gingivalis* pigment, Sci. Rep. 7 (2017) 5225 (9 page).